DIELECTRIC SPHERICAL LENS ANTENNA FOR WIRELESS MILLIMETER-WAVE COMMUNICATIONS

Reuven Shavit
Electrical and Computer Engineering Department
Ben-Gurion University of the Negev
Beer-Sheva 84105, Israel

Received 18 March 2003

ABSTRACT: *A simplified theoretical model based on geometrical optics (GO) in combination with physical optics (PO) in its vector form is used to analyze the performance of a homogeneous dielectric-sphere lens fed by a feed horn. The proposed model provides physical insight and sufficient accuracy for the initial design cycle. The computed results are also compared to measured data acquired from a prototype model and the agreement is satisfactory.* © 2003 Wiley Periodicals, Inc.
Microwave Opt Technol Lett 39: 28–33, 2003; Published online in Wiley InterScience (www.interscience.wiley.com). DOI 10.1002/mop.11117

Key words: *dielectric spherical lens; millimeter waves; wireless*

1. INTRODUCTION

The need for broadband wireless communication systems is growing, and therefore the operating frequency is gradually shifting toward millimeter-wave frequencies [1]. In recent years, this has generated increased interest in developing mm-wave antennas for indoor and outdoor applications. In addition, to cope with an increased number of users, a wide-angle scanning capability is required. In millimeter-wave frequencies, dielectric-lens antennas are good and cost-effective candidates for the task. They are effective at producing highly directive and shaped beams, and offer a range of solutions for wide-angle scanning. In most lens antenna applications, scanning is obtained by displacing the feed from its focal point and a multiple beam system is obtained by switching between displaced feeds. In the standard dielectric lens, scanning is limited to few beamwidths due to the phase aberration error caused by the displacement of the feed from the perfect focal point. Many attempts have been made to improve the scanning capability of dielectric lenses; most noticeably, the work of Shinn [2] and Rotman [3], which developed the concept of a zoned thin spherical lens to increase the wide scan capabilities beyond that of regular lenses. Even though such a design is limited in its scanning to 20°–30°. An alternative and attractive solution to the scanning problem is the design of a spherical lens, which concentrates the incident field to a focal point. Scanning is obtained by displacing the feeds on an arch around the spherical lens and, due to the perfect symmetry of the system, there are no scanning losses. One deficiency of the dielectric spherical lens is its lack of a perfect focal point. The Luneburg lens [4] is an improvement. It is spherical and, as such, has wide scanning capabilities; it also has a perfect focal point due to a continuous variation of its internal dielectric constant. In practice, the Luneburg lens, is made of a few spherical concentric shells with varying dielectric constant, which makes it less attractive due to fabrication problems and high production cost. Accordingly, the homogeneous spherical lens alternative was revisited to obtain an optimum design. The use of a homogeneous spherical dielectric lens as an antenna was first suggested and analyzed by Bekefi et al. [5], who employed GO and scalar diffraction theory. Such an analysis has its limitations and does not provide information on system losses. The exact solution of the problem of scattering from a spherically stratified Luneburg microwave lens using spherical wave functions was derived by Sanford [6] and its solution using dyadic Green's function was formulated by Mosallaei et al. [7]. The solution of a hemispherical dielectric lens fed by a double-slot feed, which is a derivation from the spherical dielectric lens, is described in [8].

This paper revisits the analysis of Bekefi et al. [5] for a homogeneous spherical dielectric lens and improves its theory by using GO combined with PO in its vector form. This method has been applied successfully to determine the radiation characteristics of various other dielectric lenses as discussed in [1, 9, 10]. The analysis uses the vector-field distribution on the lens surface to compute the radiation pattern and the system losses (spillover, tapering, phase, external reflection, and dielectric). In addition, the field in the focal region of the lens is computed to obtain a better physical insight into the design of the optimized feed for the system. The analysis provides an acceptable engineering accuracy with a shorter design cycle time, compared to the exact solution or the numerical solution using an FDTD algorithm. This statement is correct, especially for lenses with large diameters. The accuracy of the computed results with this theory is compared to numerical results obtained by simulation with a commercial software utilizing an FDTD algorithm and to measured data acquired on a prototype model, and their agreement is satisfactory.

2. THEORY

The basic geometry of the spherical lens antenna is shown in Figure 1. A dielectric sphere of radius a, dielectric constant ε_r, and loss tangent tan δ is illuminated by a y-polarized rectangular feed horn with aperture dimensions a_h and b_h. The distance between the feed-horn aperture phase center and the lens center is denoted by s. For the sake of simplicity, we define two sets of coordinate systems local coordinate system of the feed (x', y', z') or (r', η, φ) and global coordinate system (x, y, z) or (r, θ, ϕ) in cartesian or polar coordinates, respectively. The radiated spherical wave of the feed illuminates the lens (point P_1) and is collimated by the lens. The radiation pattern of the system is determined by the field distribution on the lens surface (point P_2).

2.1. Radiation Pattern

Throughout the analysis, it is assumed that the lens is illuminated by a rectangular feed horn. The feed horn aperture and its flare angle are small enough, such that the phase error caused by the flare angle can be disregarded. Accordingly, the incident field at the entrance point P_1 on the lens, can be approximated by [11]:

$$\underline{E}^i_{p1} = C\,\frac{e^{-jk_0r'}}{r'}\,[f_E(\eta)\sin\varphi\,\underline{1}_\eta + f_H(\eta)\cos\varphi\,\underline{1}_\varphi], \tag{1}$$

where $C = 2Z_0a_h^2b_h/\pi\lambda^2\,(1 + \beta_{10}/k_0)$ with $k_0 = 2\pi/\lambda_0$, $Z_0 = 120\ \pi$ the characteristic impedance in free space and β_{10} the propagation constant of the TE_{10} mode in the rectangular waveguide of the feed horn. $f_E(\eta)$ and $f_H(\eta)$ are the E- and H-plane feed horn patterns and are expressed by

$$f_E(\eta) = \frac{1 + \beta_{10}/k_0\cos\eta}{1 + \beta_{10}/k_0}\,\frac{\sin(k_0b_h/2\sin\eta)}{k_0b_h/2\sin\eta};\quad f_H(\eta) = \left(\frac{\pi}{2}\right)^2\frac{\cos\eta + \beta_{10}/k_0}{1 + \beta_{10}/k_0}\,\frac{\cos(k_0a_h/2\sin\eta)}{[(\pi/2)^2 - (k_0a_h/2\sin\eta)^2]}. \tag{2}$$

In the following, GO is used to obtain the field distribution on the lens surface (exit point P_2). The incident field is decomposed into its TE and TM components at point P_1. The reflection coefficients

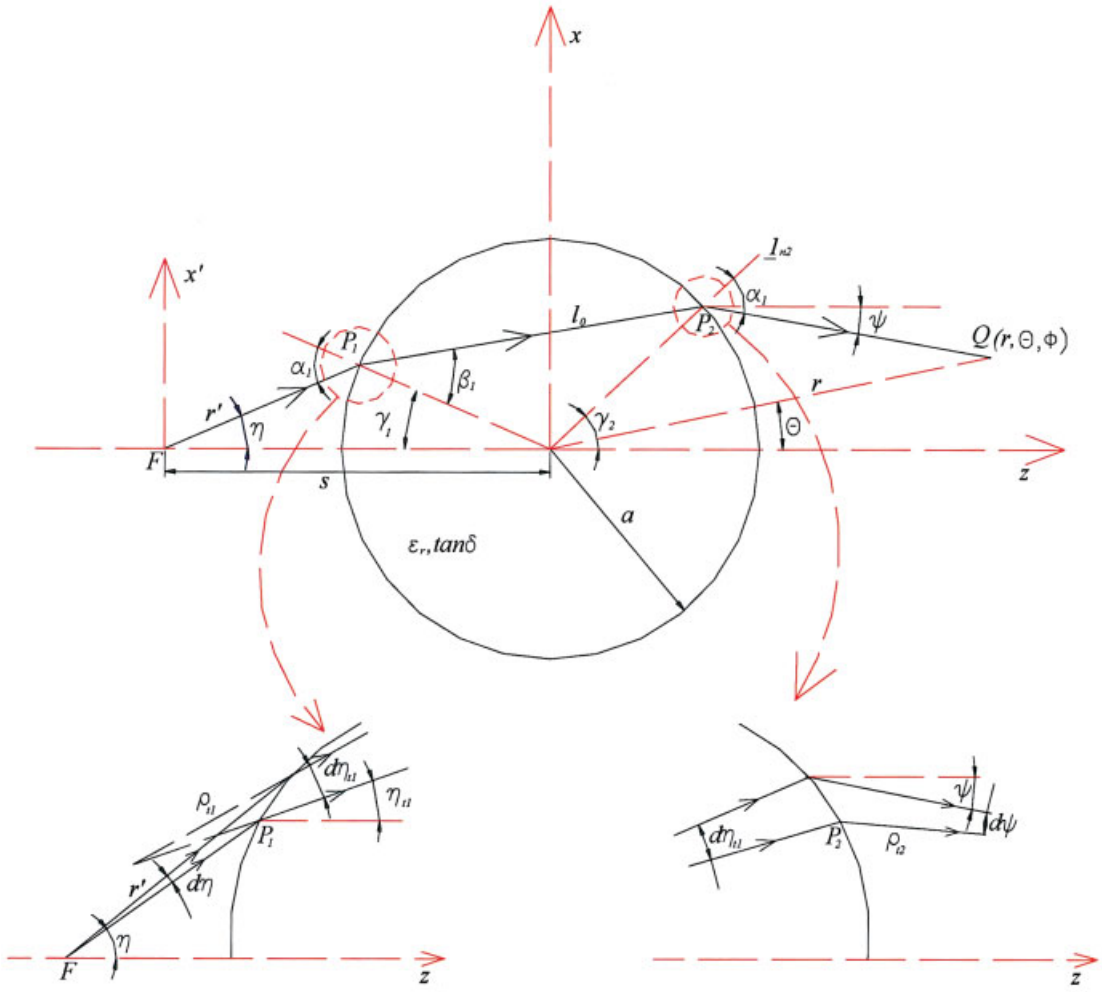

Figure 1 Dielectric sphere lens geometry and the ray tracing scheme. [Color figure can be viewed in the online issue, which is available at www.interscience.wiley.com.]

at the incident point P_1 can be found in [11] and are reproduced here as follows:

$$\Gamma_{\mathrm{TE}} = \frac{\cos\alpha_1 - \sqrt{\varepsilon_r - \sin^2\alpha_1}}{\cos\alpha_1 + \sqrt{\varepsilon_r - \sin^2\alpha_1}},$$

$$\Gamma_{\mathrm{TM}} = \frac{\varepsilon_r\cos\alpha_1 - \sqrt{\varepsilon_r - \sin^2\alpha_1}}{\varepsilon_r\cos\alpha_1 + \sqrt{\varepsilon_r - \sin^2\alpha_1}}, \tag{3}$$

in which $\alpha_1 = \sin^{-1}(s/a \sin\eta)$. The transmitted power density in the lens, can be derived based on the GO's energy conservation principle in a tube [12] (see Fig. 1). The power balance is valid for both TE- and TM-wave contributions. After some algebraic manipulations, it can be shown that the resulting field at point P_2 for the TE component of the field is

$$|\underline{E}^{t2}_{\mathrm{TE}}| = Cf_H(\eta)\frac{\rho_{t1}}{r'(\rho_{t1}+l_0)}(1-|\Gamma_{\mathrm{TE}}|^2)\cos\varphi, \tag{4}$$

and for the TM component

$$|\underline{E}^{t2}_{\mathrm{TM}}| = Cf_E(\eta)\frac{\rho_{t1}}{r'(\rho_{t1}+l_0)}(1-|\Gamma_{TM}|^2)\sin\varphi. \tag{5}$$

The electrical phase of the field at P_2 is k_0L_t and is determined by the summation of the optical lengths FP_1 and P_1P_2 (see Fig. 1). Thus,

$$k_0L_t = k_0(s\cos\eta - a\cos\alpha_1 + 2a\sqrt{\varepsilon_r}\cos\beta_1). \tag{6}$$

The dielectric losses in the lens can be approximated, if ε_r is replaced by $\varepsilon_r(1 - j\tan\delta)$ in Eq. (6). Moreover, the combination of Eqs. (4) and (5) yields the total field distribution on the lens surface at P_2, given by

$$\underline{E}^{t2} = (|\underline{E}^{t2}_{\mathrm{TE}}|\underline{1}_\varphi - |\underline{E}^{t2}_{\mathrm{TM}}|\underline{1}_\psi)e^{-jk_0L_t},$$

$$\underline{H}^{t2} = \frac{1}{Z_0}(|\underline{E}^{t2}_{\mathrm{TE}}|\underline{1}_\psi + |\underline{E}^{t2}_{\mathrm{TM}}|\underline{1}_\varphi)e^{-jk_0L_t}. \tag{7}$$

Given the field distribution of Eq. (7) on the lens surface s_a, the actual far-field radiation pattern $\underline{E}_Q(r, \theta, \phi)$ can be computed using the equivalence theorem and PO [11]:

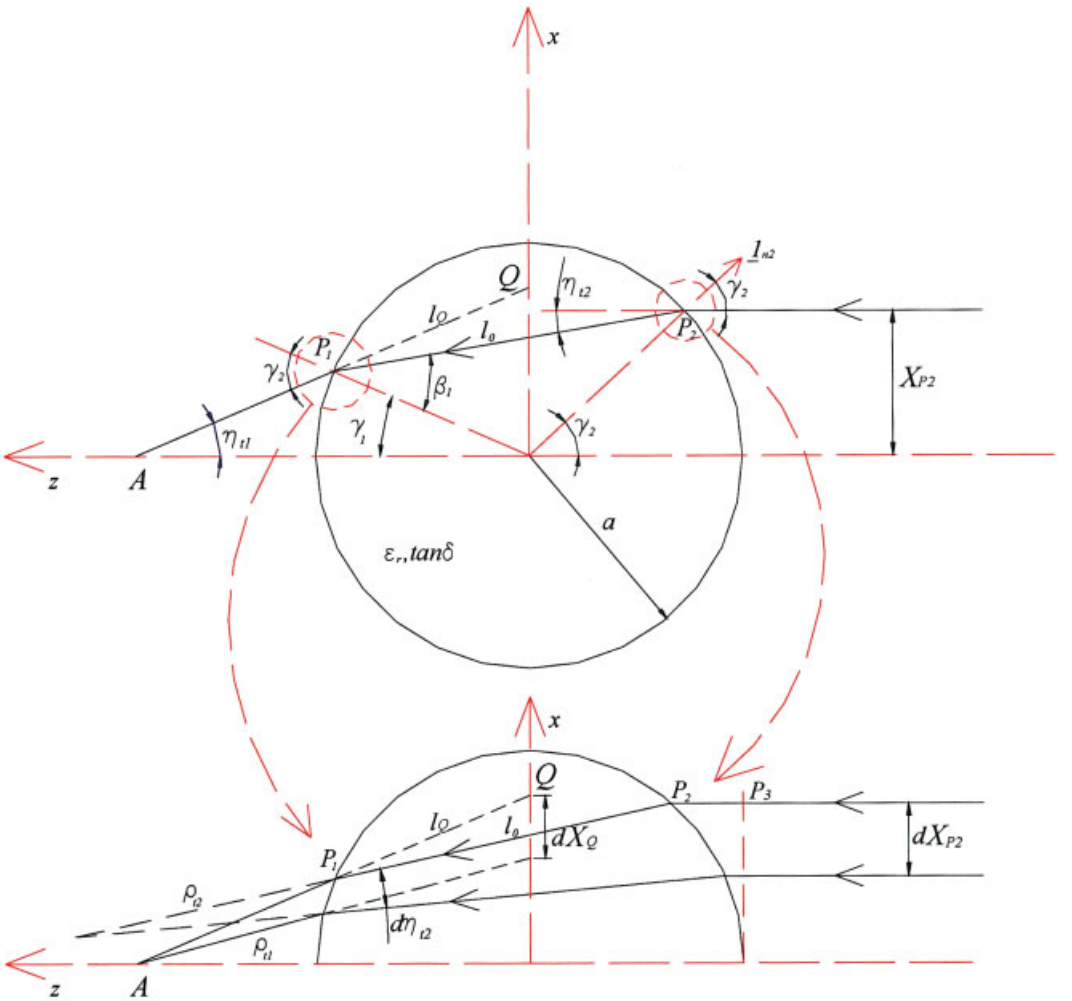

Figure 2 Dielectric sphere lens geometry and the ray tracing scheme for an incident planar wave. [Color figure can be viewed in the online issue, which is available at www.interscience.wiley.com.]

$$\underline{E}_Q(r,\,\theta,\,\phi) = j\,\frac{e^{-jk_0r}}{2\lambda r}\left\{\int_{s_a}\left[Z_0(\underline{1}_{n2}\times\underline{H}^{t2})\times\underline{1}_r + (\underline{1}_{n2}\times\underline{E}^{t2})\right] \times \underline{1}_r e^{jk_0a\underline{1}_{n2}\cdot\underline{1}_r}\,ds\right\}, \tag{8}$$

in which

$$\underline{1}_r = \sin\theta\cos\phi\underline{1}_x + \sin\theta\sin\phi\underline{1}_y + \cos\theta\underline{1}_z,$$

$$\underline{1}_{n2} = \sin\gamma_2\cos\varphi\underline{1}_x + \sin\gamma_2\sin\varphi\underline{1}_y + \cos\gamma_2\underline{1}_z. \tag{9}$$

2.2. Gain Computation

In this paper, it is assumed that the feed horn is excited by a TE_{10} mode. If we ignore the feed horn aperture phase error, the total radiated power by the feed horn, P_a can be computed by integration of the Poynting vector over the feed horn aperture, such that

$$P_a = \frac{1}{2}\int_{-a_h/2}^{a_h/2}\int_{-b_h/2}^{b_h/2} E_{y'}H_{x'}dx'dy' = \frac{Z_0\beta_{10}}{2\lambda\pi}a_h^3b_h. \tag{10}$$

Consequently, by definition the lens antenna gain [11] is

$$G = \frac{4\pi}{P_a}\frac{1}{2Z_0}\left|\underline{E}_Q(r,\,0,\,0)\right|^2r^2 \tag{11}$$

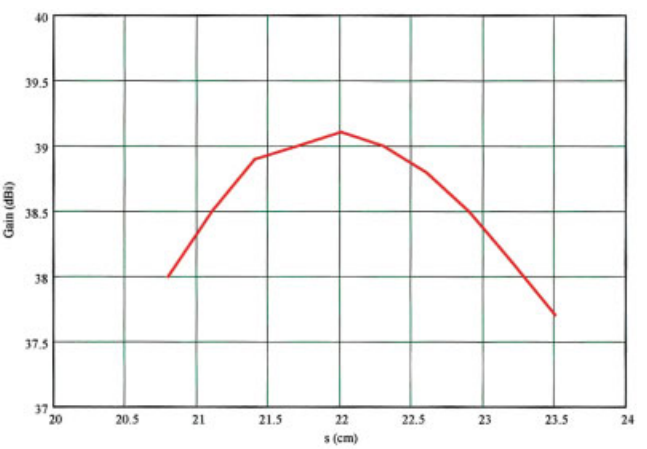

Figure 3 Antenna gain dependence on feed horn location on the antenna axis (a_h = 1.1 cm, b_h = 0.9 cm). [Color figure can be viewed in the online issue, which is available at www.interscience.wiley.com.]

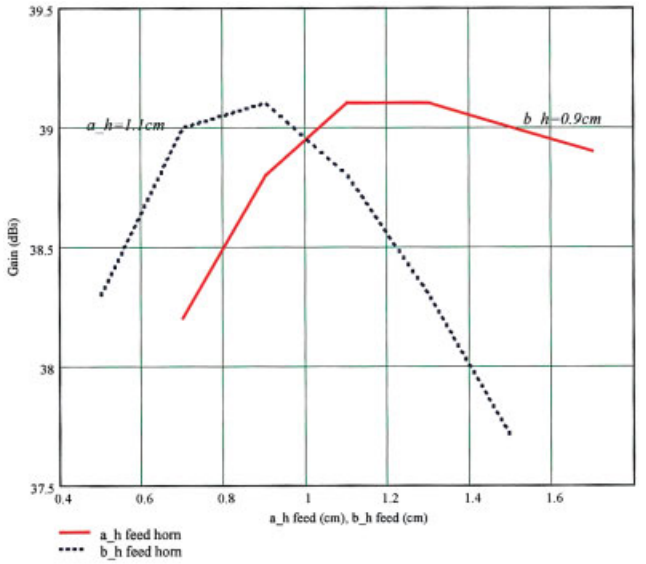

Figure 4 Antenna gain dependence on feed horn aperture dimensions for $s = 22$ cm. [Color figure can be viewed in the online issue, which is available at www.interscience.wiley.com.]

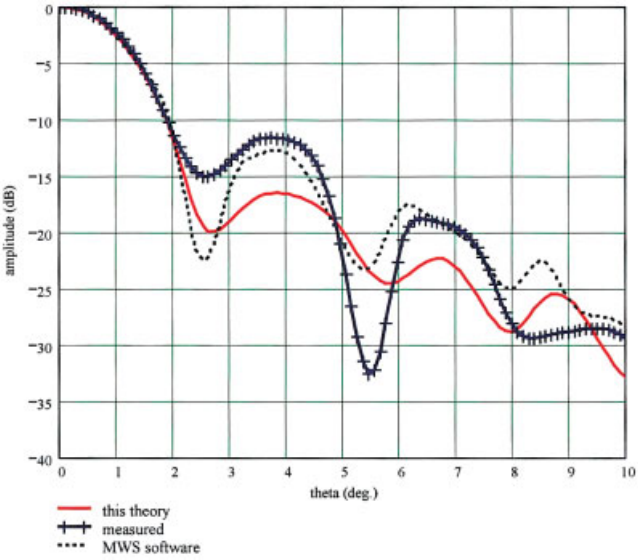

Figure 6 $E_\theta(\theta, 0)$ computed with this theory compared to results computed with MWS software (FDTD algorithm) and measured data. [Color figure can be viewed in the online issue, which is available at www.interscience.wiley.com.]

Substitution of Eqs. (8) and (10) into Eq. (11) gives the explicit expression for the gain. The expression in (11) computes the gain, including system losses, such as: feed spillover, taper losses, phase losses, dielectric losses, and the reflection losses at the lens input surface. This computation does not include the multiple internal-reflection losses, which are neglected throughout the current derivation and are presumed negligible. The effect of internal reflections can be found in [10]. This turns to be a valid assumption, if ε_r is relatively low.

2.3. *Field Distribution in the Focal Region*

The dielectric sphere lens system does not have a perfect focal point due to the phase aberration error in the system. Therefore, it is beneficial to compute the field distribution (phase and amplitude) in the focal region in order to match it to the feed horn field for maximum gain performance. The problem is solved using a hybrid model of GO and diffraction theory. Figure 2 shows the geometry of a planar wave with unit field amplitude and TE or TM polarization. The field distribution on the lens surface is computed at P_1 using GO and it is back-projected on the xy plane to obtain a virtual circular aperture. Given the field distribution on the projected aperture through the lens center, the axial field distribution on the lens' z axis can be computed using the diffraction theory. x_{P2} denotes the x coordinate of the incident ray parallel to z axis and x_Q denotes the coordinate of the field back projected on xy plane. P_1P_2 is the optical path length in the lens. In a fashion similar to that described in the previous section, GO can be utilized to derive the power density distribution on the lens surface at the output point P_1. The electrical phase ϕ_Q of the back projected field on the xy plane is determined by the summation of the optical lengths P_3P_2, P_2P_1, and P_1Q (see Fig. 2) to obtain

$$\phi_Q = k_0 a\left(1 - \cos\gamma_2 + 2\sqrt{\varepsilon_r}\cos\beta_1 - \frac{\cos\gamma_1}{\cos\eta_{t1}}\right). \qquad (12)$$

The amplitude of the electric field distribution on the xy plane can be determined in a similar fashion to that described in Eqs. (4) and (5) to yield the total field distribution, $E_Q(x_Q)$ in the xy plane, given by

$$E_Q(\rho_Q) = \frac{\rho_{t1}}{\rho_{t2}}\frac{(\rho_{t2} + l_0)}{(\rho_{t1} + l_Q)}(1 - |\Gamma_{\mathrm{TE,TM}}|^2)\sqrt{\cos\eta_{t1}}\, e^{-j\phi_Q}, \qquad (13)$$

where $\rho_Q = \sqrt{x_Q^2 + y_Q^2}$. Once the field distribution on the xy plane is known, the diffraction integral [12] can be employed to compute the field distribution on the z axis in the focal region of the lens, such that

$$E_A(z) = jk_0 a\int_{s_Q} |E_Q| e^{-j\phi_Q}\frac{e^{-jk_0R}}{R}\cos(\theta - \eta_{t1})ds_Q, \qquad (14)$$

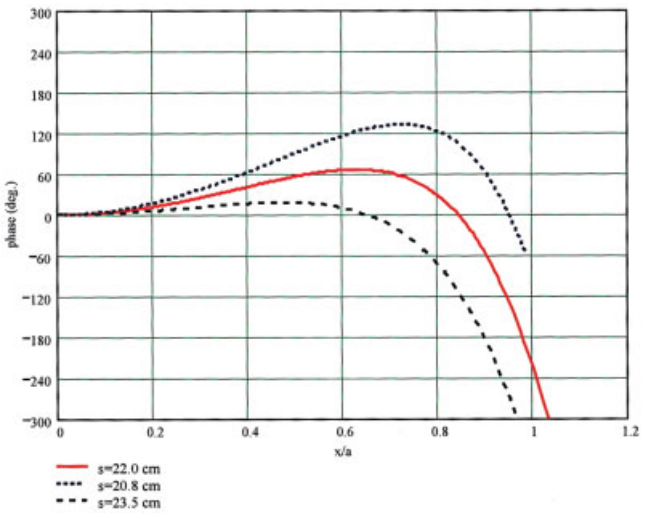

Figure 5 The field phase distribution on a plane in front of the lens. [Color figure can be viewed in the online issue, which is available at www.interscience.wiley.com.]

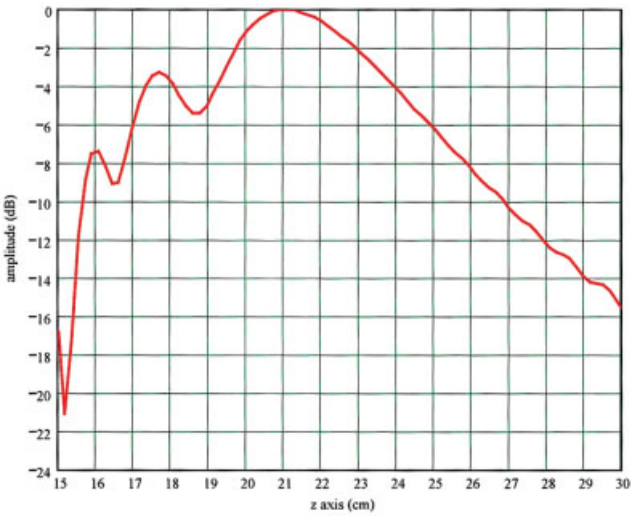

Figure 7 Field distribution dependence on the z axis (in close proximity to the focal point) for an incident plane wave. [Color figure can be viewed in the online issue, which is available at www.interscience.wiley.com.]

in which $ds_Q = \rho_Q d\rho_Q d\varphi$, $R = \sqrt{\rho_Q^2 + z^2}$, and $\theta = \tan^{-1}(\rho_Q/z)$.

3. NUMERICAL RESULTS

As a test case, a dielectric spherical lens made of Teflon ($\varepsilon_r = 2.02$, $\tan\delta = 0.0006$) and 30 cm in diameter was considered, and a prototype with this dimension was built and tested. The operating frequency was 38 GHz. The lens was illuminated by a rectangular feed horn. Figure 3 shows the antenna gain's [computed by Eq. (11)] dependence on the distance s from the lens center for a typical feed horn with aperture dimensions $a_h = 1.1$ cm and $b_h = 0.9$ cm. Optimum performance is achieved for $s = 22$ cm, which results in a gain value of 39.1 dBi (with aperture efficiency of 57%). The gain was computed using Microwave Studio (MWS) commercial software from CST via an FDTD algorithm for electromagnetic (EM) simulation, which resulted in 38.7 dBi (with aperture efficiency of 52%). In the simulation with MWS, the feed was simulated as an actual horn with aperture dimensions a_h and b_h and a flare angle of 10°. Figure 4 shows a parameter study performed on the feed aperture dimensions a_h and b_h to determine the optimum feed dimensions for maximum gain. The results show that the optimum performance is obtained using a feed with aperture dimensions $a_h = 1.1$ cm and $b_h = 0.9$ cm, and at a distance of $s = 22$ cm from the lens center. In this configuration, the feed observation angle $\eta_{\max}$ is equal to 42.9° (see Fig. 1).

Figure 5 shows the field phase distribution on a plane in front of the lens or back-projected on the xy plane for various s distances of the feed from the lens center. One can observe that at the optimum distance $s = 22$ cm, the phase distribution is somewhat balanced between negative and positive phases. Variation of the frequency from 35–41 GHz for a system with the optimum parameters ($a_h = 1.1$ cm, $b_h = 0.9$ cm, $s = 22$ cm) results in a gain variation from 38.5–39.5 dBi. This change is equivalent to an aperture efficiency variation of 58–53%, which demonstrates that the system has a wide frequency bandwidth. Moreover, a 5% variation in the spherical lens diameter with all other parameters constant results in a drop in the aperture efficiency to 45–48%, which is also an indication of a robust system. Variation of the lens dielectric constant to $\varepsilon_r = 2.1$ and $\varepsilon_r = 1.9$, resulted in aperture efficiency of 49% and 42%, respectively. Figure 6 shows a comparison between the radiation pattern, $E_\theta(\theta, 0)$ of the dielectric spherical lens with the optimized feed described before [computed using Eq. (8)], the radiation pattern computed using the commercial software MWS and measured data. Similar results are obtained in other planes. One can observe a good agreement in the main beam with deviations in the sidelobe levels. This difference can be attributed to mechanisms not accounted in the current model (internal reflections, creeping waves, lateral-wave excitation near the critical angle of incidence in the internal part of the lens). The agreement between the MWS numerical results and the measured data is good. The price paid in the better agreement using MWS simulation software is CPU time: two min for the proposed model compared to more than 10 h on a 1.7-GHz PC Pentium IV, with 2-Gb RAM for the MWS computation.

Figure 7 shows the field distribution on the lens axis in the vicinity of the optimum location of the feed ($s = 22$ cm) for an incident planar wave. One can notice a relatively mild drop in the field distribution in the vicinity of the optimum feed location, which is an indication of a non-distinctive focal point and a possible cause for losses inflicted in the system, if a standard feed horn is used to collect the energy from the lens. This distribution gives also an indication of a possible improvement of the system efficiency by using a traveling wave feed such as a dielectric rod or linear radial slot array feed with a near field distribution similar to that shown in Figure 7. In applications where the antenna compactness and number of beams is not an issue, it would be enough to increase the system efficiency by using a second lens together with the feeding horn to correct the direction of the rays emerging from the spherical lens and direct them to a perfect focus [12].

4. SUMMARY

This paper presents a theoretical analysis of the radiation and gain characteristics for a homogeneous spherical dielectric lens illuminated by a rectangular feed horn. The analysis is based on GO to obtain the amplitude and phase distribution on the lens surface and then PO analysis is used to determine the gain and radiation pattern of the lens system. In addition, the analysis is extended to compute the field distribution in the focal region of the antenna to obtain a physical insight on the most appropriate feed to optimize the gain of the antenna. A typical test case in mm wave is considered to study the effectiveness of the proposed analysis. The computed results are compared to computations performed on a commercial simulation software using an FDTD algorithm and to measured data acquired on a prototype lens 30 cm in diameter, and the agreement is satisfactory. The advantage of the suggested model compared to the FDTD model is especially emphasized for lenses with large diameters, which require very long time of computation and large amounts of memory.

ACKNOWLEDGMENT

The authors wish to express their gratitude to A. Anis for running the simulations on the MWS commercial software, performing the measurements, and for engaging in many helpful discussions on the subject during the course of this work.

REFERENCES

1. C.A. Fernandes and J. Fernandes, Performance of lens antennas in wireless indoor millimeter-wave applications, IEEE Trans Microwave Theory Tech MTT-47 (1999), 732–737.
2. D.H. Shinn, The design of a zoned dielectric lens for wide angle scanning, Marconi Rev XVIII (1955), 37–47.
3. W. Rotman, Analysis of an EHF aplanatic zoned dielectric lens antenna, IEEE Trans Antennas Propagat AP-32 (1984), 611–617.

4. R.K. Luneburg, Mathematical theory of optics, Brown University, Providence, RI, 1944.
5. G. Bekefi and G.W. Farnell, A homogeneous dielectric sphere as a microwave lens, Canadian J Phys 34 (1956), 790–803.
6. J.R. Sanford, Scattering by spherically stratified microwave lens antennas, IEEE Trans Antennas Propagat AP-5 (1994), 690–698.
7. H. Mosallaei and Y. Rahmat-Samii, Nonuniform Luneburg and two-shell lens antennas: Radiation characteristics and design optimization, IEEE Trans Antennas Propagat AP-1 (2001), 60–69.
8. D.F. Filipovic, S.S. Gearhart, and G.M. Rabeiz, Double-slot antennas on extended hemispherical and elliptical silicon dielectric lenses, IEEE Trans Microwave Theory Tech 41 (1993), 1738–1749.

OMNIDIRECTIONAL PLANAR DIPOLE-ARRAY ANTENNA FOR 2.4/5.2-GHz WLAN ACCESS POINTS

Kin-Lu Wong, Jeng-Wen Lai, and Fu-Ren Hsiao
Department of Electrical Engineering
National Sun Yat-Sen University
Kaohsiung 80424, Taiwan

Received 14 March 2003

ABSTRACT: *An omnidirectional dual-band planar dipole-array antenna suitable for application in 2.4/5.2-GHz WLAN access points is presented. The dipole-array antenna is a linear array and comprises three back-to-back dipole elements with the first two elements operating in the 5.2-GHz band and the third one operating in the 2.4-GHz band. The proposed array antenna is narrow in width (12 mm in this design), and good omnidirectional radiation with gain variations less than 2 dBi for both the 2.4- and 5.2-GHz bands is obtained. In addition, the an-*

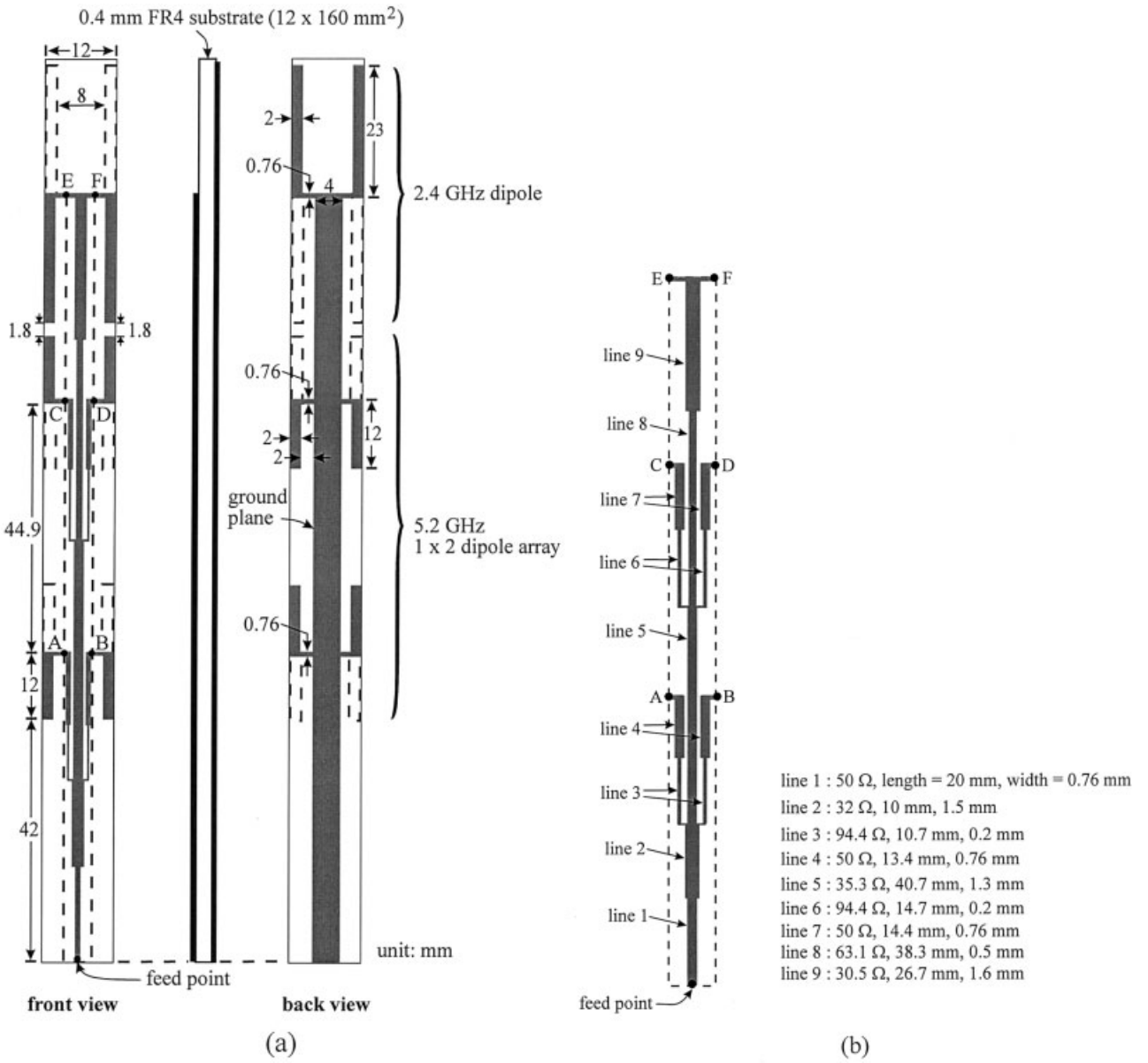

Figure 1 (a) Geometry of the proposed omnidirectional planar dipole array antenna for 2.4/5.2-GHz WLAN operation; (b) dimensions of the feeding network